


8-2018

# Evaluation of drug-loaded gold nanoparticle cytotoxicity as a function of tumor tissue heterogeneity.

Hunter Allan Miller  
*University of Louisville*

Follow this and additional works at: <https://ir.library.louisville.edu/etd>

 Part of the [Computer Sciences Commons](#), [Nanomedicine Commons](#), [Other Applied Mathematics Commons](#), [Other Biomedical Engineering and Bioengineering Commons](#), [Pharmacology Commons](#), and the [Toxicology Commons](#)

---

## Recommended Citation

Miller, Hunter Allan, "Evaluation of drug-loaded gold nanoparticle cytotoxicity as a function of tumor tissue heterogeneity." (2018). *Electronic Theses and Dissertations*. Paper 3050.  
<https://doi.org/10.18297/etd/3050>

This Master's Thesis is brought to you for free and open access by ThinkIR: The University of Louisville's Institutional Repository. It has been accepted for inclusion in Electronic Theses and Dissertations by an authorized administrator of ThinkIR: The University of Louisville's Institutional Repository. This title appears here courtesy of the author, who has retained all other copyrights. For more information, please contact [thinkir@louisville.edu](mailto:thinkir@louisville.edu).

EVALUATION OF DRUG-LOADED GOLD NANOPARTICLE CYTOTOXICITY AS  
A FUNCTION OF TUMOR TISSUE HETEROGENEITY

By

Hunter Allan Miller

B.S., Murray State University, 2018

A Thesis

Submitted to the Faculty of the  
School of Medicine of the University of Louisville

in Partial Fulfillment of the Requirements

For the Degree of

Master of Science

In Pharmacology and Toxicology

Department of Pharmacology and Toxicology

School of Medicine

Louisville, Kentucky

August 2018



EVALUATION OF DRUG-LOADED GOLD NANOPARTICLE CYTOTOXICITY AS  
A FUNCTION OF TUMOR TISSUE HETEROGENEITY

By  
Hunter Allan Miller  
B.S., Murray State University, 2016

A Thesis Approved on

July 11, 2018

by the following Thesis Committee:

---

Hermann Frieboes, Ph.D.

---

Jill Steinbach-Rankins, Ph.D.

---

Ayman El-Baz, Ph.D.

---

Eric Rouchka, D.Sc.

---

Joshua Hood, M.D., Ph.D.

## DEDICATION

This thesis is dedicated to my father, mother, and sister

Mr. Daniel Miller,

Mrs. Sherry Miller,

and

Mrs. Holly Wood

whose encouragement and support has pushed me to achieve my goals.

## ACKNOWLEDGEMENTS

I would like to thank my principal advisor Dr. Hermann Frieboes, for his guidance and commitment to my graduate education. I also thank the faculty and staff of the Department of Pharmacology and Toxicology for their support. I also thank my family for their patience and support while I was busy with course work and research, and I look forward to their continued support for the remainder of my studies. Finally, I would like to thank the School of Interdisciplinary and Graduate Studies at the University of Louisville School of Medicine for funding my opportunity to pursue this research.

## ABSTRACT

### EVALUATION OF DRUG-LOADED GOLD NANOPARTICLE CYTOTOXICITY AS A FUNCTION OF TUMOR TISSUE HETEROGENEITY

Hunter A. Miller

July 11, 2018

The inherent heterogeneity of tumor tissue presents a major challenge to nanoparticle-mediated drug delivery. This heterogeneity spans from the molecular to the cellular (cell types) and to the tissue (vasculature, extra-cellular matrix) scales. Here we employ computational modeling to evaluate therapeutic response as a function of vascular-induced tumor tissue heterogeneity. Using data with three-layered gold nanoparticles loaded with cisplatin, nanotherapy is simulated with different levels of tissue heterogeneity, and the treatment response is measured in terms of tumor regression. The results show that tumor vascular density non-trivially influences the nanoparticle uptake and washout, and the associated tissue response. The drug strength affects the proportion of proliferating, hypoxic, and necrotic tissue fractions, which in turn dynamically affect and are affected by the vascular density. This study establishes a first step towards a more systematic methodology to assess the effect of vascular-induced tumor tissue heterogeneity on the response to nanotherapy.

## TABLE OF CONTENTS

	PAGE
ACKNOWLEDGEMENTS.....	iv
ABSTRACT.....	v
LIST OF FIGURES.....	vii
INTRODUCTION.....	1
METHODS AND MATERIALS.....	4
Nanoparticle Synthesis and Characterization.....	4
Experimental Cytotoxicity Data.....	4
Computational Modeling.....	5
RESULTS.....	14
Experimental Data.....	14
Simulation of Heterogeneous Tumor Growth.....	14
Calibration of Drug Effect.....	16
Simulation of Nanoparticle-Mediated Drug Delivery.....	17
DISCUSSION.....	27
REFERENCES.....	30
CURRICULUM VITAE.....	36



## LIST OF FIGURES

FIGURE	PAGE
1. Tumor nodules growing in time with different levels of vascular induced tissue heterogeneity .....	16
2. Characterization of tumor tissue heterogeneity .....	17
3. Simulated tumor growth in avascular ( <i>in vitro</i> ) conditions.....	18
4. Heterogeneously vascularized tumors treated with cisplatin-loaded nanoparticles .....	20
5. Nanoparticle concentration within tumor tissue .....	22
6. Drug release from nanoparticles within the first 4 hrs. ....	23
7. Intratumoral nanoparticle and intratumoral vascular drug AUC values .....	24
8. Minimum tumor radii achieved at each IC50 drug strength as a function of the intratumoral vascular drug AUC for each level of tissue heterogeneity.....	25
9. Minimum tumor radius achieved during therapy as a function of Drug strength and tissue heterogeneity.....	26
10. Minimum tumor radii achieved during treatment as a function of drug strength dependent on the viable tissue fraction and intratumoral vascular density.....	26

## INTRODUCTION

Although nanoparticle-mediated drug delivery offers the promise of more targeted and effective treatment of cancer, few of the myriad of formulations evaluated in the laboratory have reached clinical application. Major hurdles have included concerns about toxicity, lower than expected efficacy, and off-target effects (Miele, Spinelli et al. 2012). In particular, the tumor microenvironment can present a formidable barrier that hinders the transport of drug molecules as well as nano-sized vehicles (Primeau, Rendon et al. 2005, Hait and Hambley 2009, Warren 2013). In order to be effective, nanoparticle-mediated drug delivery needs to utilize the vascular network to preferentially reach the tumor site and penetrate into the cancerous tissue to establish cytotoxic concentrations, avoid uptake by the reticulo-endothelial system (RES), diffuse through the extra-cellular matrix (ECM) mesh of proteins, remain close or be uptaken by the cancer cells, and efficiently release the payload of drug molecules to achieve cytotoxicity. To address these requirements and increase the efficacy of chemotherapy, nanoparticles can be functionalized with various compounds to help reduce systemic distribution and avoid intrinsic cellular resistance mechanisms (Koziara, Whisman et al. 2006, Bertrand, Wu et al. 2014). Yet uncoordinated angiogenic stimuli by proliferating and hypoxic cancer cells induce a heterogeneous vascular response, characterized by tortuous vessels with abnormal structure

and irregular flow (Izuishi, Kato et al. 2000, Minchinton and Tannock 2006). The inadequacy of the vascular network promotes intra-tumoral tissue regions with heterogeneous proliferative, hypoxic, and apoptotic states, while severely impairing the transport of and the response to systematically-administered drugs and nanoparticles.

The efficacy of nanoparticles in cancer treatment is typically evaluated with *in vitro* and *in vivo* experimental models, which are indispensable for pre-clinical evaluation. However, *in vitro* models lack key features of cancerous tissue found *in vivo*, including a vascular network, while *in vivo* models present challenges due to systemic interactions which may not be necessarily easily teased apart. As a complement to these experimental venues, computational simulation of cancer nanotherapy has aimed to provide the capability for system-level analysis (Frieboes, Sinek et al. 2006, Decuzzi, Pasqualini et al. 2009, Godin, Driessen et al. 2010, Li, Al-Jamal et al. 2010, Li and Reineke 2011, Li, Panagi et al. 2012, van de Ven, Wu et al. 2012, Gao, Li et al. 2013, Kaddi, Phan et al. 2013, Li, Czynszczon et al. 2013, van de Ven, Abdollahi et al. 2013, Wu, Frieboes et al. 2014). In particular, we have recently studied via mathematical modeling the extravasation, uptake, and distribution of nanoparticles subject to heterogeneous tumor tissue and vascular conditions (Curtis, England et al. 2016, Curtis, Rychahou et al. 2016, Reichel, Curtis et al. 2017).

The distribution and penetration of 2- and 3-layered gold nanoparticles were recently evaluated *in vitro* (England, Priest et al. 2013) and *in vivo* (England 2015). The purpose of these nanoparticles was to increase chemotherapy efficacy (England 2015, England, Gobin et al. 2015) via enhanced distribution and penetration into tumor tissue. The 3-layer gold nanoparticles were functionalized with phosphatidylcholine,

hexadecanethiol and high-density lipoprotein (England, Priest et al. 2013). Computational modeling was implemented (Curtis, England et al. 2016) to simulate the performance of these nanoparticles *in vivo* given measurements *in vitro*, with the goal to begin bridging the gap from the pre-clinical to the clinical setting. The model parameters were set from experimental measurements with 2D and 3D cultures of A549, H358, and PC9 Non-Small Cell Lung Cancer (NSCLC) cells (England, Priest et al. 2013, England 2015).

In this study, computational simulation is employed to evaluate the role of vascular density-induced heterogeneity on the distribution of 3-layered gold nanoparticles in tumor tissue and the associated drug release. Small metastatic lesions are simulated in a well vascularized organ, such as the lung, and cisplatin is used as the model drug. The nanoparticle effectiveness is analyzed by calculating fractions of control for tumors of various blood vessel densities after bolus administration of the drug loaded nanoparticles. Tumor therapy is simulated with various drug inhibitory concentrations calibrated to achieve a 50% reduction in tumor size (IC50) at four timepoints (24hr, 48hr, 72hr, 96hr) post treatment initiation. This work represents a first step towards quantifying tumor response to drug-loaded nanoparticles based on vascular-network induced tissue heterogeneity.

## MATERIALS AND METHODS

### Nanoparticle Synthesis and Characterization

Three-layered nanoparticles were previously created in (England, Priest et al. 2013). Briefly, citrate-stabilized gold nanoparticles were synthesized by reducing chloroauric acid with trisodium citrate (Frens 1973). The first layer applied was 1-Hexadecanethiol (TL), followed by phosphatidylcholine (PC), and then HDL. Nanoparticles were characterized via extinction spectra using ultraviolet-visible (UV-Vis) spectrometry, zeta potential measurements, DLS (dynamic light scattering) to determine hydrodynamic size (intensity distribution) in solution, determination of shape and size with scanning electron microscopy, and confirmation of presence of lipids on the particle cores using a Fourier transform infrared (FTIR) instrument. Cisplatin (7.5 mg) was then added to the nanoparticles in solution and allowed to react for 2 h (England, Priest et al. 2013).

### Experimental Cytotoxicity Data

As described in (England, Priest et al. 2013), A-549 cells were maintained in standard culture conditions, and used to form tumor spheroids. Cytotoxicity was first measured in 3D cell culture with free drug at varying concentrations (1024, 256, 64, 16, 4, 1, 0.25, 0.0625  $\mu\text{M}$ ) for 48 h. The spheroids were exposed to varying concentrations of drug-loaded nanoparticles calculated by considering two parameters: (1) the loading

efficiency from HPLC data showing the exact concentration of drug encapsulated onto the nanoparticles (England 2015) and (2) the percent of drug released over the 48-hour period.

## Computational Modeling

### 1. Tumor Growth

The tumor growth component is based on (Macklin, McDougall et al. 2009, Wu, Friboes et al. 2013), in which tumor tissue is denoted by  $\Omega$  and its boundary by  $\Sigma$ . Tumor tissue is divided into three regions: a proliferating region where cells have sufficient oxygen and nutrients to proliferate, a hypoxic region where cells have sufficient oxygen and nutrients to survive but insufficient for proliferation, and a necrotic region where cells lack sufficient oxygen and nutrients for survival. The non-dimensionalized tumor growth velocity follows Darcy's Law [48]:

$$\mathbf{v}_c = -\mu\nabla P + \chi_E \nabla E \quad \text{[Equation 1]}$$

where  $\mu$  is cell-mobility,  $P$  is oncotic pressure,  $\chi_E$  is haptotaxis, and  $E$  is the density of the extracellular matrix (ECM). Refer to (Macklin, McDougall et al. 2009) for a more detailed description of  $E$  and  $\chi_E$ . The overall tumor growth can be associated with the rate of volume change by assuming that the cell density within the proliferating region remains constant:

$$\nabla \cdot \mathbf{v}_c = \lambda_p \quad \text{[Equation 2]}$$

where  $\lambda_p$  is the non-dimensionalized net proliferation rate (described below).

### 2. Angiogenesis

The angiogenesis component is based on (McDougall, Anderson et al. 2006) to represent blood flow, vascular leakage and vascular network remodeling resulting from wall shear stress and mechanical stress imposed by the tumor tissue as it changes in time. Briefly, as the tumor grows within a vascularized environment, the tissue has access to oxygen and nutrients diffusing from the vasculature. The interstitial flow of oxygen and nutrients is influenced by tissue pressure and by distance from the nearest vessel. Refer to (Macklin, McDougall et al. 2009, Wu, Frieboes et al. 2013) for a more detailed description of the angiogenesis model.

### 3. Transport of oxygen and nutrients

Oxygen and nutrients  $\sigma$  are transported to the tumor from the location of extravasation from the vasculature. The extravasation rates  $\lambda_{ev}^{\sigma} = \lambda_{neo}^{\sigma}$  and  $\lambda_{ev}^{\sigma} = \lambda_{pre}^{\sigma}$  represent the rate that  $\sigma$  are supplied from the neo- and pre-existing vasculature, respectively. These substances, which diffuse with a coefficient  $D_{\sigma}$ , are taken up by both host tissue cells and tumor cells with rates  $\lambda_{tissue}^{\sigma}$ ,  $\lambda_{tumor}^{\sigma}$ , and  $q_s$  and decay with rate  $\lambda_N^{\sigma}$  in the necrotic region. Under steady-state conditions, the formulation of oxygen and nutrient uptake and decay is (Macklin, McDougall et al. 2009, van de Ven, Wu et al. 2012, Wu, Frieboes et al. 2014):

$$0 = \nabla \cdot (D_{\sigma} \nabla \sigma) + \lambda_{ev}^{\sigma}(\mathbf{x}, t, \mathbf{1}_{vessel}, p_i, \sigma, h) - \lambda^{\sigma}(\sigma)\sigma \quad [\text{Equation 3}]$$

where  $\mathbf{x}$  is position,  $t$  is time,  $\mathbf{1}_{vessel}$  is the characteristic function for the vasculature (equals 1 at vessel locations and 0 otherwise),  $p_i$  is interstitial pressure, and  $h$  is the hematocrit in the vascular network [48]. Extravasation is modulated by the extravascular interstitial

pressure  $p_i$ , scaled by the effective pressure  $p_e$  with the weight of the convective transport component of small molecules,  $k_{p_i}$  (van de Ven, Wu et al. 2012):

$$\lambda_{ev}^\sigma = \bar{\lambda}_{ev}^\sigma \mathbf{1}_{vessel}(\mathbf{x}, t) \left( \frac{h}{\bar{H}_D} - \bar{h}_{min} \right)^+ \left( 1 - k_{p_i} \frac{p_i}{p_e} \right) (1 - \sigma) \quad [\text{Equation 5}]$$

$\bar{H}_D$  and  $h_{min}$  are constants which represent the normal and minimum hematocrit necessary for oxygen extravasation, respectively.  $\bar{\lambda}_{ev}^\sigma$  represents the constant transfer rate from pre-existing and tumor-induced vessels.

#### 4. Transport of nanoparticles

Nanoparticle transport  $s$  through the tumor tissue is simulated from the point of extravasation from the vasculature. The uptake rate of nanoparticles by host and tumor cells is  $\bar{\lambda}_{uptake}^s$  (van de Ven, Wu et al. 2012, Wu, Frieboes et al. 2014):

$$\frac{\partial s}{\partial t} = \nabla \cdot (D_s \nabla s) + \lambda_{ev}^s(\mathbf{x}, t, \mathbf{1}_{vessel}, p_i, s) - \bar{\lambda}_{uptake}^s s \quad [\text{Equation 6}]$$

Under the assumption that the transfer rate  $\bar{\lambda}_{ev}^s$  from both pre-existing and tumor-induced vessels is constant, nanoparticle extravasation is: represented by (van de Ven, Wu et al. 2012, Wu, Frieboes et al. 2014):

$$\lambda_{ev}^s = \bar{\lambda}_{ev}^s \mathbf{1}_{vessel}(\mathbf{x}, t) \left( 1 - k_{p_i} \frac{p_i}{p_e} \right) \left( \frac{C_t^s}{\bar{C}^s} - s \right) \quad [\text{Equation 7}]$$

where diffusion of particles into the tumor tissue is modulated by the interstitial pressure (van de Ven, Wu et al. 2012). Particle extravasation is assumed to be  $C_t^s = \bar{C}^s e^{-at}$ , where



$\bar{C}^s$  is the initial concentration (van de Ven, Wu et al. 2012). The extravasation of particles is concentration dependent, simulating first order kinetics. The decay constant  $\alpha$  is measured from previous *in vivo* experiments, in which the particle half-life is estimated to be 12 hours (England, Huang et al. 2015). The diffusivity of the particles was calibrated from the combination of charge and size properties based on measurements obtained *in vitro* (England, Priest et al. 2013).

## 5. Transport of drug

Drug  $G$  is released at the point of extravasated particles and diffuses through the tumor tissue with the coefficient  $D_G$ . The rate  $\bar{\lambda}_{decay}^G$  combines the effects of drug uptake by tumor and normal cells and the wash-out from the interstitial space, and reflects the half-life of the drug (Curtis, England et al. 2016):

$$\frac{\partial G}{\partial t} = \nabla \cdot (D_G \nabla G) + \lambda_{release}^G(t, s) - \bar{\lambda}_{decay}^G G \quad [\text{Equation 8}]$$

The drug release  $\lambda_{release}^G$  from the particles is represented by (Curtis, England et al. 2016):

$$\lambda_{release}^G = s C_t^G \quad [\text{Equation 9}]$$

$C_t^G$  is the release of drug which is fitted in time to follow the results obtained from *in vitro* experiments in [38]. The drug release rate thus combines the effect of particle concentration and drug release profile. All diffusion equations have the boundary condition  $\frac{\partial B}{\partial n} = 0$  where  $B$  is the diffusible substance.

## 6. Drug effect on tumor

Cisplatin is a cell cycle dependent drug, and thus its cytotoxic effect is only exerted on proliferating cells. Drug effect is included into the proliferation term  $\lambda_p$  where  $\bar{\lambda}_{effect}$  is the rate of drug-induced cell death (Wu, Frieboes et al. 2014):

$$\lambda_p = \begin{cases} 0 & \text{outside the tumor} \\ \lambda_M \sigma (1 - \bar{\lambda}_{effect} G) - \lambda_A & \text{in proliferating tissue} \\ 0 & \text{in hypoxic tissue} \\ -G_N & \text{in necrotic tissue} \end{cases} \quad [\text{Equation 10}]$$

where  $\lambda_A$  is the apoptosis rate,  $\lambda_M$  is the mitosis rate, and  $G_N$  is the non-dimensional rate of volume loss in the necrotic tumor core (it is assumed that cellular debris is constantly degraded and the fluid is removed (Wu, Frieboes et al. 2014)). This pharmacodynamic model assumes that cell proliferation and apoptosis rates are similar before and after drug therapy. Cell death is assumed to be instantaneous.

## 7. Calibration of Rate of Drug-Induced Cell Death

The model parameters for oxygen, drug effect and tumor growth were calibrated using data obtained experimentally with NSCLC tumor spheroids to find an 48hr IC50 for simulated avascular spheroids (*in vitro* simulations) (England, Priest et al. 2013). A detailed description of the *in vitro* experiments used to calibrate the simulations can be found in (Curtis, England et al. 2016), which includes the synthesis, functionalization, characterization, drug loading, and drug release of the nanoparticles and cytotoxicity experiments in 2D and 3D cell culture. Since the concentration of NP's and drug were not changed among the four IC50's, the free drug concentration after 48 h of exposure was calculated based on the data from our previous study (Curtis, England et al. 2016). Then, the 24hr, 72hr, and 96hr IC50 avascular treatment drug concentrations were scaled by the

same proportion as the change in drug effect. The trapezoid method was used to calculate the corresponding AUC's to quantify the avascular IC50's.

## 8. Tumor Tissue Heterogeneity

The values for drug-induced cell death used for the avascular IC50's were employed in therapy simulations with vascularized lesions (simulations of *in vivo* condition). To link the differences in drug effect to the effects of heterogeneous vascularization density, the *in vivo* simulations used the same nanoparticle concentration in a bolus dose as was needed in the *in vitro* simulations to achieve the IC50. All tumors grown in host tissue with the same pre-existing vessel densities but different oxygen thresholds for hypoxia and necrosis were grown to the same initial radius of 0.56mm. *In vivo* simulations were run for a sufficient amount of time to obtain the smallest tumor radii following NP bolus injection and were used to compare the efficacy of cisplatin-loaded nanoparticles among the various cases. The tumor blood vessel density was calculated by dividing vessel surface area (vessel length x vessel cross sectional area) by the tumor area. The main tumor, nanoparticle, and drug parameters and their values are summarized in **Table 1**.

<b>Parameter</b>	<b>Value</b>	<b>Reference</b>
Tumor proliferation rate	1 day <sup>-1</sup>	Measured in (Curtis, England et al. 2016)
Oxygen diffusivity	1 (*)	(Wu, Frieboes et al. 2013)
Oxygen transfer rate from vasculature	5 (*)	(Wu, Frieboes et al. 2013)

Oxygen uptake rate by proliferating tumor cells	1.5 (*)	(Wu, Frieboes et al. 2013)
Oxygen uptake rate by hypoxic tumor cells	1.3 (*)	(Wu, Frieboes et al. 2013)
Oxygen uptake rate by tumor microenvironment	0.12 (*)	(Wu, Frieboes et al. 2013)
Oxygen decay rate	0.35 (*)	(Wu, Frieboes et al. 2013)
NP extravasation from angiogenic vs. normal vessels	10	Estimated
NP diffusivity	0.3 (*)	(England, Priest et al. 2013)
NP decay	12hr half-life	Estimated
CDDP diffusivity	0.6 (*)	Estimated
CDDP drug effect	27, 9.45, 5.6, 4.0 (for 24, 48, 72, and 96 h IC50)	Calibrated to experimental data
CDDP decay rate	0.5hr half-life	(Leighl 2012)
CDDP release profile from NP		Measured in (England 2015)

CDDP <i>in vitro</i> IC50 (48 h) for A549 cells (spheroid)	15.9 ± 1.2 μM	Measured in (Curtis, England et al. 2016)
--	---------------	---

**Table 1:** Computational model main parameters and associated values. All other model parameters are as in (Wu, Frieboes et al. 2013). (\*) Value is rescaled by the square of the simulation system characteristic length (1 cm) and divided by the system characteristic time (1 sec) multiplied by the oxygen diffusivity (Nugent and Jain 1984) ( $1 \times 10^{-5} \text{ cm}^2 \text{ s}^{-1}$ ). CDDP: cisplatin; NP: 3-layered gold nanoparticles characterized in (England, Priest et al. 2013, England 2015, Curtis, England et al. 2016).

Four levels of tissue heterogeneity were obtained, respectively labeled “very low,” “low,” “medium,” and “high,” by varying the angiogenesis-induced tissue vascularization based on the response to tumor angiogenic factors (TAF) that were in proportion to the tumor tissue hypoxic and necrotic levels. The values for these levels are defined in **Table 2**. The hypoxic threshold defines the oxygen level at which tissue becomes hypoxic (quiescent but still viable) and ceases to proliferate, while the necrotic thresholds defines the oxygen level at which the tissue becomes necrotic (dead).

Level of Tissue Heterogeneity	Tumor hypoxic threshold	Tumor necrotic threshold
VERY LOW	0.305	0.300
LOW	0.405	0.400
MEDIUM	0.485	0.480
HIGH	0.575	0.570

**Table 2:** Definition of levels of tumor tissue heterogeneity based on the thresholds for inducing hypoxia and necrosis. The values for HIGH are based on the previously calibrated tumors simulated in (van de Ven, Wu et al. 2012, Curtis, England et al. 2016).

## RESULTS

### Experimental data

The 3-layer gold nanoparticles were previously characterized as having a maximum wavelength of 5.35 nm, a hydrodynamic diameter of  $80.2 \pm 12.4$  nm, and a zeta potential of -6 mV (Curtis, England et al. 2016). The cisplatin loading efficiency was  $78.9 \pm 0.7\%$  (Curtis, England et al. 2016). The nanoparticles released  $59.1 \pm 2.0\%$  of drug within the first 3 hours,  $76.7 \pm 1.84$  within 48 h, and  $78.9 \pm 2.1$  by 96 h (England 2015).

### Simulation of heterogeneous tumor growth

Tumors were first grown under the conditions of VERY LOW, LOW, MEDIUM and HIGH heterogeneity as defined in **Table 2** to the same radius (0.566 mm) before treatment. The simulated tumors during the initial growth phase are shown in **Figure 1**. Depending on the level of heterogeneity, this growth took varying amounts of time, with the HIGH case taking the longest (22.7 simulated days). The tissue heterogeneity is characterized in **Figure 2** as a function of the tumor radius. While the intra-tumoral vessel density initially increased for the VERY LOW and LOW cases, it plateaued for radii beyond 0.40 mm (**Figure 2A**). In contrast, the density for MEDIUM and HIGH conditions decreased for radii below 0.31 and 0.28  $\mu\text{m}$ , respectively, before becoming larger. The proliferative tissue fraction corresponding to these vascular densities indicates that for a

radius of 0.566 mm right before start of treatment, these fractions were being maintained at 96, 82, 68, and 55% for VERY LOW, LOW, MEDIUM and HIGH conditions, respectively (**Figure 2B**). At this radius, the hypoxic tissue fractions were correspondingly lower, at 2.4, 4.8, 10.0, and 20.2% (**Figure 2C**), while the necrotic fraction values were 1.2, 12.6, 21.9, and 25.3%, respectively. Compared to the more stable values maintained for the proliferating and hypoxic as the tumor radius increased, the necrotic fractions (**Figure 2D**) (except for the VERY LOW condition) exhibited an initial steep increase followed by a gentle decline past 0.350  $\mu\text{m}$  as the proliferating portion slowly started gaining in value.



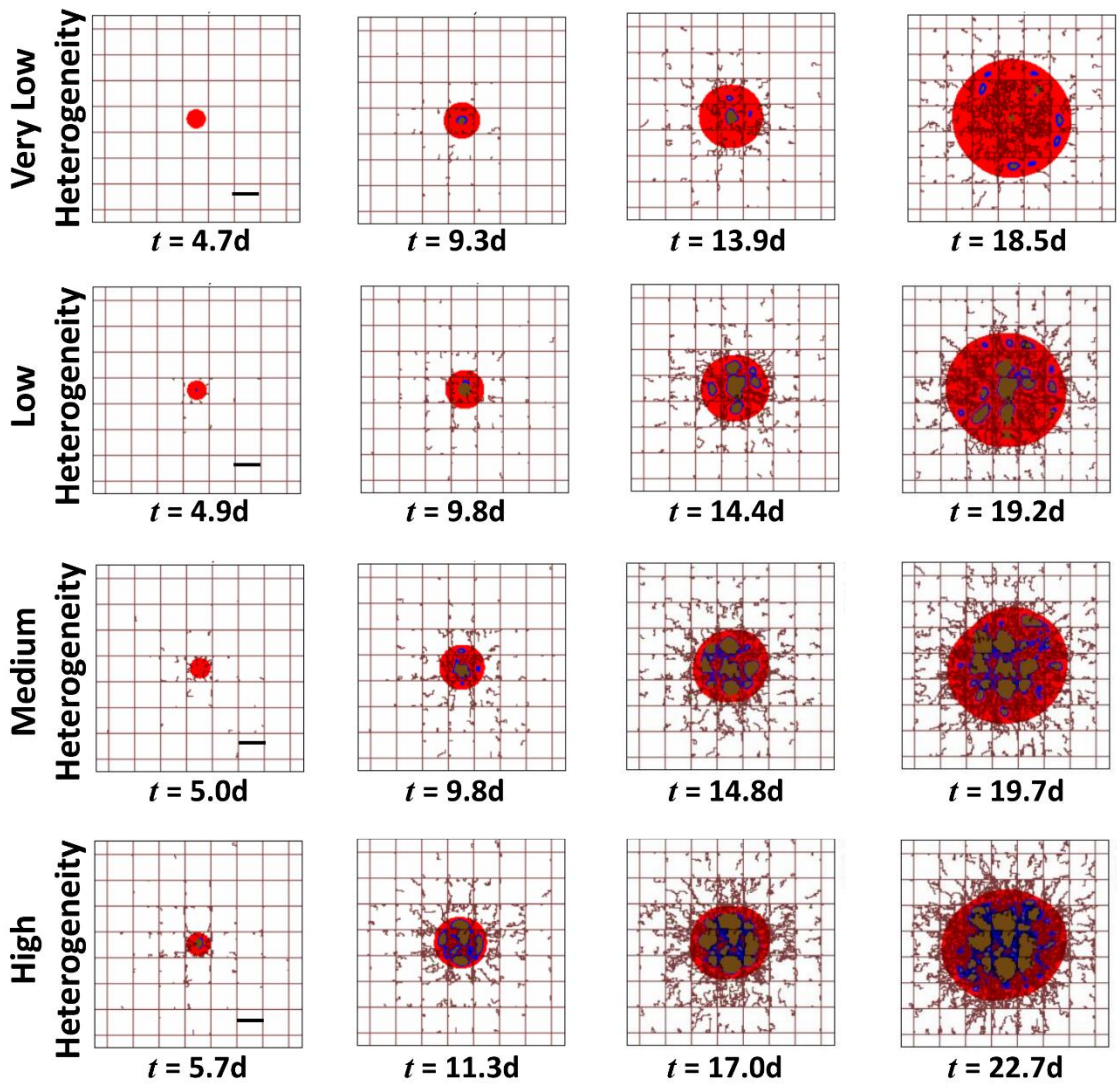


**Figure 1.** Simulation of tumor nodules growing in time with different levels of vascular-induced tissue heterogeneity. Red color denotes the proliferating region, blue indicates hypoxia, and brown means necrosis. The pre-existing capillary grid is shown as rectangular lines along with irregular sprouts growing from them due to the angiogenesis process. Bar: 250  $\mu\text{m}$ .

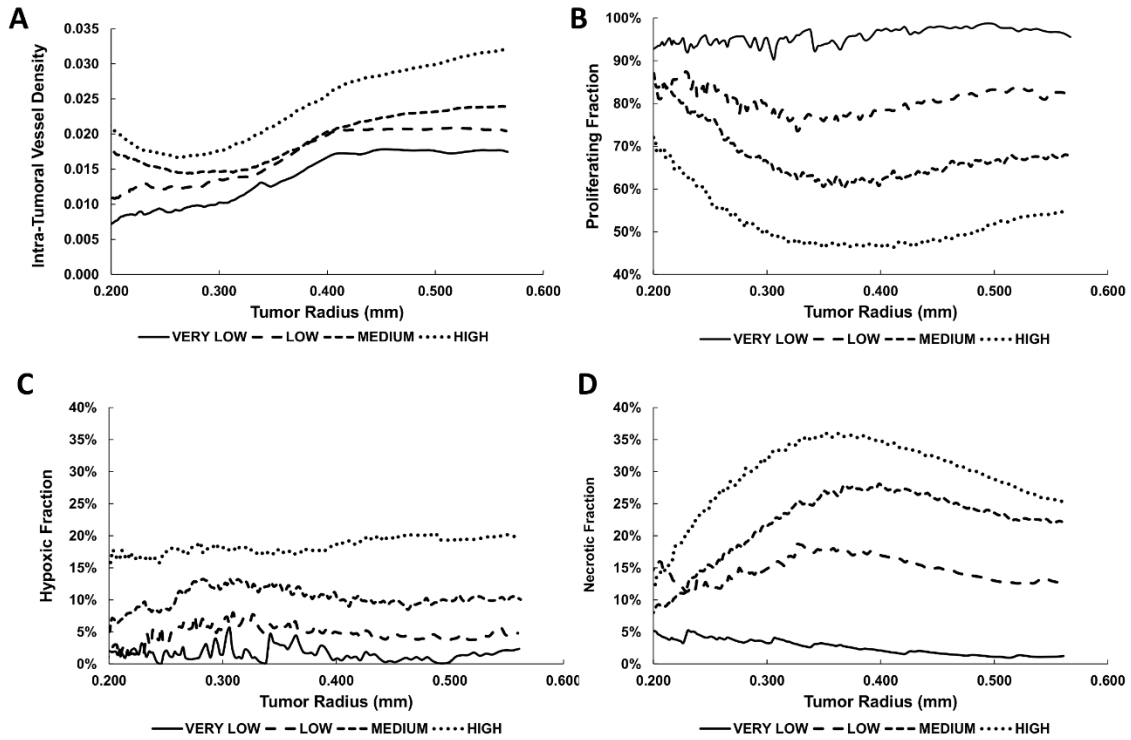


**Figure 2.** Characterization of tumor tissue heterogeneity. (A) Intra-tumoral vascular density; (B) Proliferating fraction; (C) Hypoxic fraction; (D) Necrotic fraction.

### Calibration of drug effect

A simulated tumor growing in the dish *in vitro*, surrounded by plentiful oxygen and nutrients, is shown in **Figure 3A**. This tumor was exposed after 30 d to drug *in silico* for 48 h to determine the value for the drug effect  $\bar{\lambda}_{effect}$  to achieve a 50% reduction in tumor size (the “IC50”) (**Figure 3B**). This value was then assigned the units of the drug concentration to achieve the same regression with the tumor spheroids in the experiments *in vitro* (Curtis, England et al. 2016). A range of area-under-the-curve values were obtained, as shown in **Table 3**.

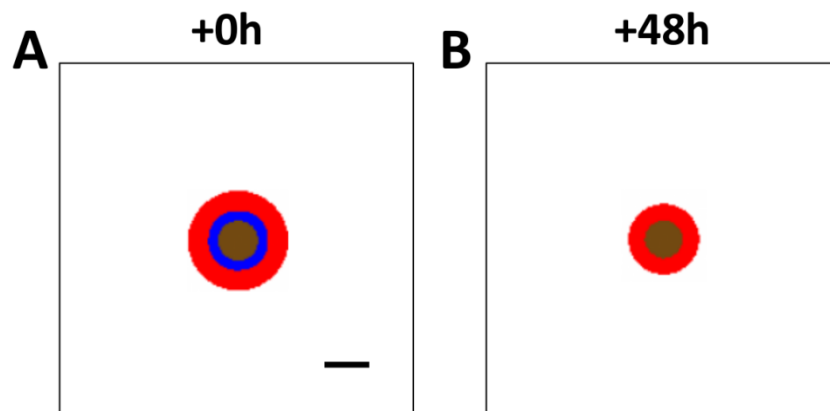


**Figure 3.** Simulated tumor growing in avascular conditions in vitro. Red: proliferating tissue; blue: hypoxic tissue; brown: necrotic tissue. Bar: 250  $\mu\text{m}$ .

IC50 Range of Time (h)	AUC ( $\mu\text{M}\cdot\text{h}$ )
24hr IC50	1082
48hr IC50	760
72hr IC50	676
96hr IC50	644

**Table 3.** Area-under-curve (AUC) calculated for four different ranges of time for a simulated tumor spheroid growing in *in vitro* conditions.

#### Simulation of nanoparticle-mediated drug delivery

Representative simulation images of vascularized tumors at the start of treatment with the various levels of heterogeneity are shown in **Figure 4**. As the heterogeneity

increases from VERY LOW to HIGH, the penetration and spatial distribution of nanoparticles and the drug released from them correspondingly becomes more heterogeneous. The deepest nanoparticle penetration is achieved with the VERY LOW case, for which the drug release is concentrated in the inner core of the tumor. In contrast, in the HIGH case the nanoparticles become stuck in the tumor periphery, unable to penetrate into the tissue. This is consistent with previous modeling work showing that tumor tissue heterogeneity leads to inhomogeneous small molecular and nanoparticle distribution, with the highest concentrations occurring on the periphery (Frieboes, Wu et al. 2013, Curtis, Wu et al. 2015). Interestingly, although in the LOW case the nanoparticles penetrate deeper, their concentration is more heterogeneously distributed than in the MEDIUM case, suggesting that the relationship between heterogeneity and nanoparticle penetration is not linear (Frieboes, Wu et al. 2013, Curtis, Wu et al. 2015).

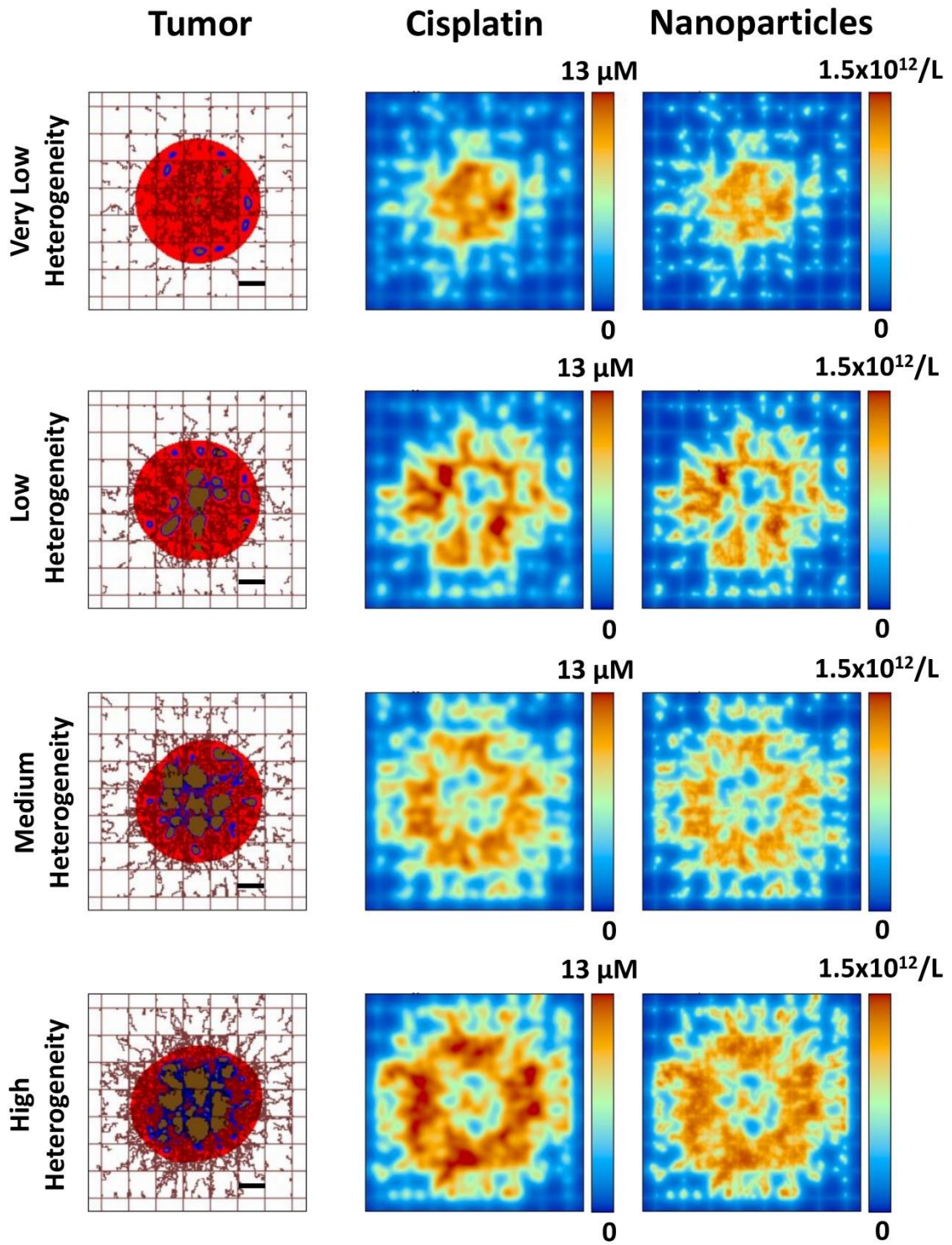


**Figure 4.** Representative simulation images of vascularized tumors with the various levels of heterogeneity shown at the start of treatment with cisplatin-loaded nanoparticles. Red: proliferating tissue; blue: hypoxic tissue; brown: necrotic tissue. Bar: 250  $\mu\text{m}$ .

The nanoparticle concentration within tumor tissue for each value of the drug strength (respectively based on 24, 48, 72, and 96 h IC<sub>50</sub> values *in vitro*) is shown in **Figure 5**. In the case of the 24 h IC<sub>50</sub> value, the concentrations are similar regardless of level of tissue heterogeneity, with an initial sharp peak at 2.5 h post-treatment initiation followed by a sharp drop to 35% of initial concentration within 4 h. The concentration then declines slowly afterwards, to 10% of initial by 30 h. For the other three drug strengths, the LOW case exhibits the highest concentration of nanoparticles overall, with 30% still in tissue after 30 h. For the 48h IC<sub>50</sub> case, the VERY LOW case retains the second highest concentration, while for both 72 and 96 h, it is similar to the MEDIUM and HIGH conditions, decreasing to 20% of initial value by 30 h. Noticeably, the nanoparticle concentrations are more heterogeneous in time for the 48 and 72 h cases, while the 24 and 96 h evince more consistent profiles. This suggests that the drug strength is also a key parameter that influences the nanoparticle concentration as the tissue responds in time to the drug, and is consistent with recent findings from an optimization model applied to this tumor model system (Chamseddine, Frieboes et al. 2018).

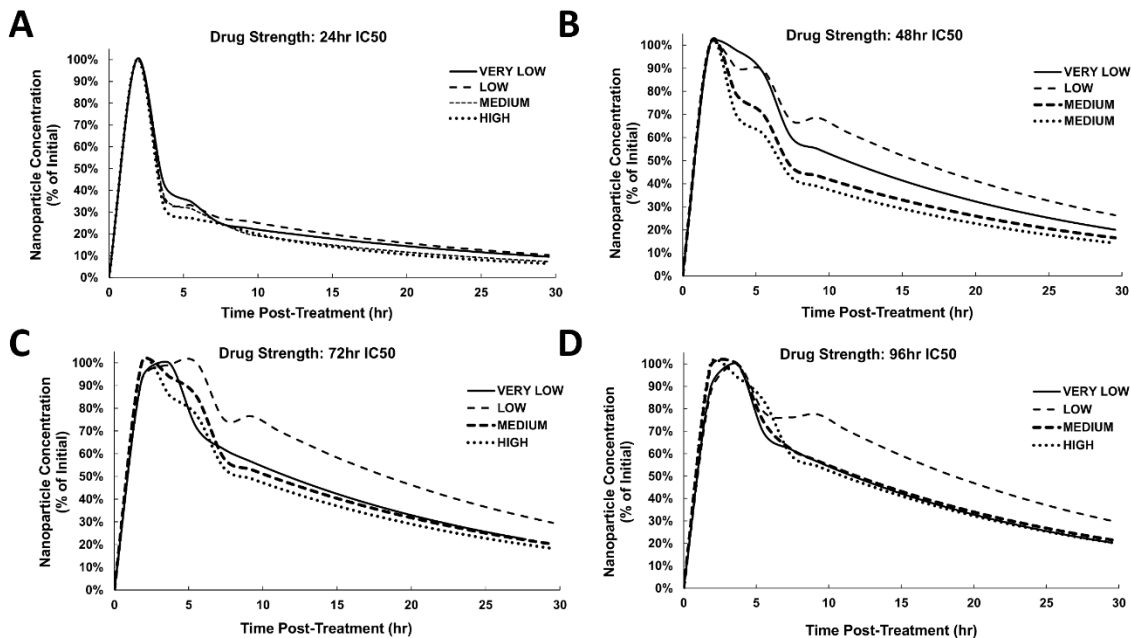


**Figure 5.** Nanoparticle concentration within tumor tissue for each value of the drug strength.

The drug release from the nanoparticles within the first 4 h for the various drug strengths is shown in **Figure 6**. Consistently, the highest concentrations were achieved for HIGH tissue heterogeneity and the lowest for the VERY LOW heterogeneity. The 24 h IC50 strength exhibited the greatest differential between the various levels of heterogeneity, at 7  $\mu\text{M}$  for HIGH and 5  $\mu\text{M}$  for VERY LOW, in contrast to the 96 h IC50, which evinced 1  $\mu\text{M}$  for HIGH and 0.75  $\mu\text{M}$  for VERY LOW.

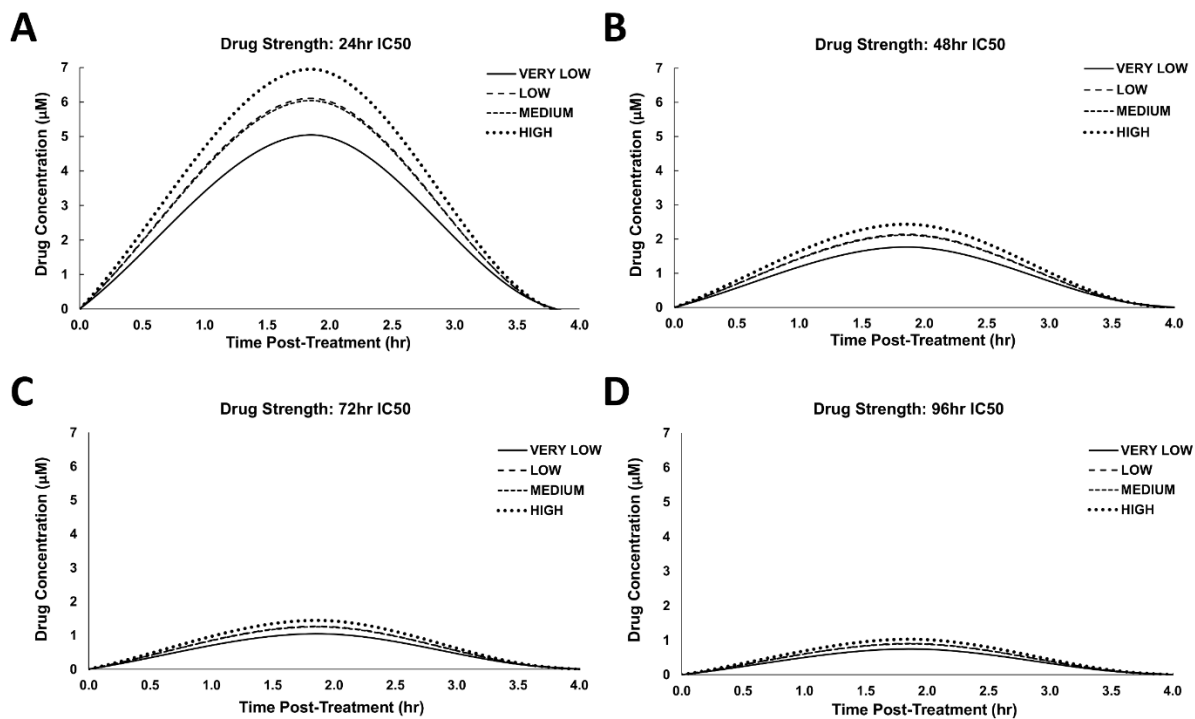


**Figure 6.** Drug release from the nanoparticles within the first 4 h for the various drug strengths.

The area-under-the-curve (AUC) for the nanoparticles within tumor tissue is shown in **Figure 7A**. Whereas the AUC for the 24 h IC50 condition declined from the VERY LOW to the HIGH heterogeneity levels, ranging from 7 to 6 %initial.h, the other three IC50 conditions had the highest values for the LOW level. At this level, the 72 h IC50 predominated overall at 17.5 %initial.h. In contrast, the highest AUC at the VERY LOW case was attained for the 48 h IC50 at 14 %initial.hr, while the highest values for the MEDIUM and HIGH conditions were for the 96 h IC50, at 15 and 13.8 %initial.h, respectively. In spite of these inhomogeneous outcomes for the nanoparticles, the intratumoral vascular AUC for the drug released from them had a more consistent pattern



across the levels of heterogeneity and drug strength (**Figure 7B**). The 24 h IC50 evinced the highest values overall, increasing from 9.6  $\mu\text{M}\cdot\text{h}$  to 13.1  $\mu\text{M}\cdot\text{h}$  for the VERY LOW and HIGH levels, respectively. The values for the other drug strengths followed the same trend but at lower values, ranging for the VERY LOW to HIGH levels at 3.5, 2.1, and 1.5  $\mu\text{M}\cdot\text{h}$  to 4.7, 2.8, and 2.0  $\mu\text{M}\cdot\text{h}$  for 48, 72, and 96 h IC50 strengths, respectively. Thus, the 96 h IC50 had the lowest drug AUC values.

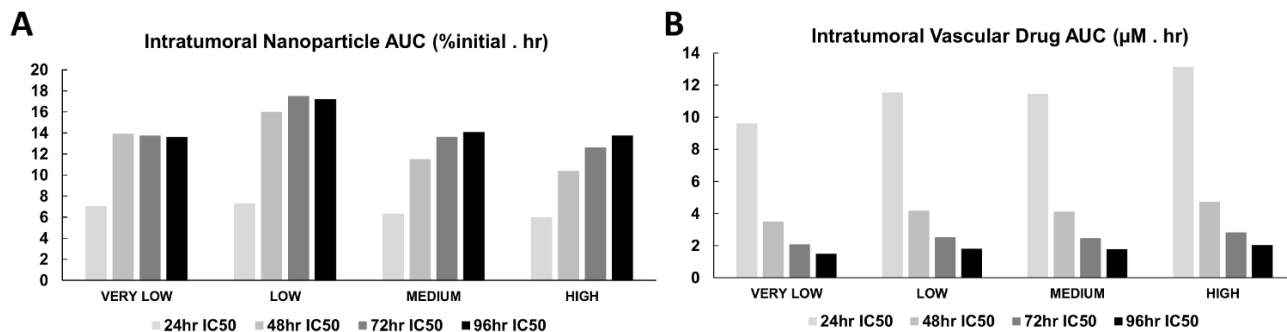


**Figure 7.** Intratumoral nanoparticle and intratumoral vascular drug AUC values.

**Figure 8** shows the minimum tumor radii achieved at each IC50 drug strength as a function of the intratumoral vascular drug AUC for each level of tissue heterogeneity. In all cases, there was a nearly linear relationship between tumor radius and AUC, with radii decreasing as the AUC values increased. The largest radius reduction was achieved by the VERY LOW case with the 24 h IC50 drug strength, yielding 52% from the initial tumor radius, while the smallest decrease at this drug strength was 41% for the MEDIUM case. On the other hand, the 96 h IC50 drug strength was equally ineffective across all levels of heterogeneity, achieving at best a 9% reduction in tumor radius. This information is summarized in **Figure 10**, highlighting the nonlinear decrease in tumor radii for the

different drug strengths across the four levels of heterogeneity. While higher drug strengths, as represented by lower IC50 values, yielded higher response, the magnitude of this response was dependent on the level of tissue heterogeneity.

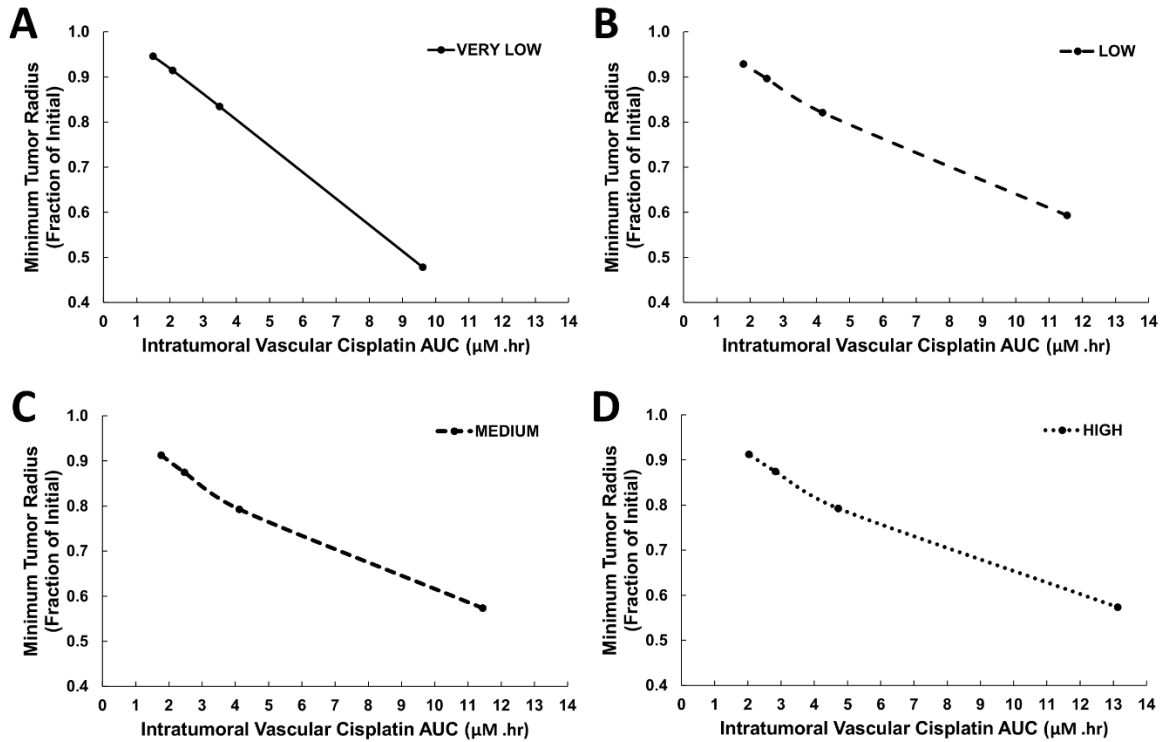


**Figure 8.** Minimum tumor radii achieved at each IC50 drug strength as a function of the intratumoral vascular drug AUC for each level of tissue heterogeneity. The points along each curve represent, from left to right, 96, 72, 48, and 24 IC50-based drug strength values.

**Figure 9** shows the minimum tumor radii as a function of drug strength dependent on the size of the tumor tissue viable (proliferating and hypoxic) fraction and intratumoral vascular density, both calculated at the start of the treatment. As expected, as the drug strength increases (represented by the IC50 values), the tumor regression is correspondingly higher. For the highest strength (24 h IC50), this regression was

maximized by higher values of the viable tumor tissue fraction (**Figure 9A**) and lower values of the intratumoral vascular density, together representing lower tumor heterogeneity (**Figure 9B**). For the other drug strengths, the regression was generally independent of this density.

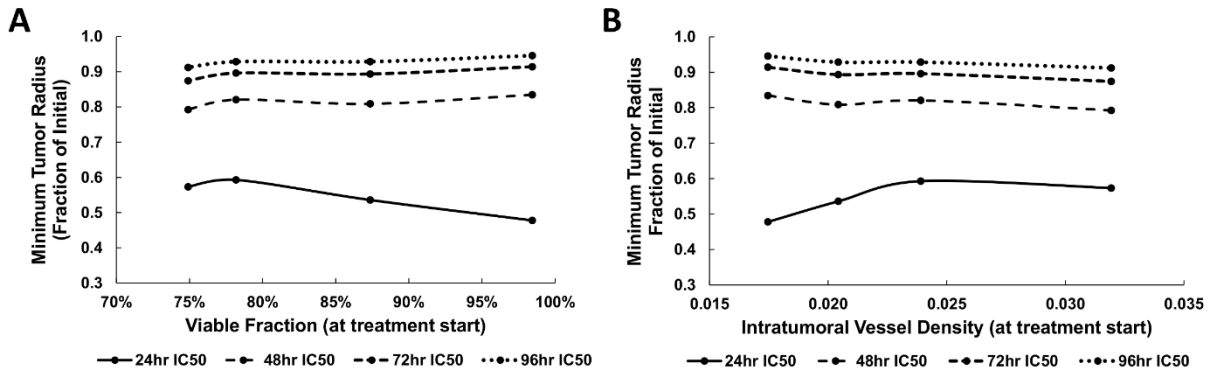


**Figure 9.** Minimum tumor radii achieved during treatment as a function of drug strength dependent on the size of the tumor tissue viable (proliferating and hypoxic) fraction and intratumoral vascular density, both calculated at the start of the treatment.

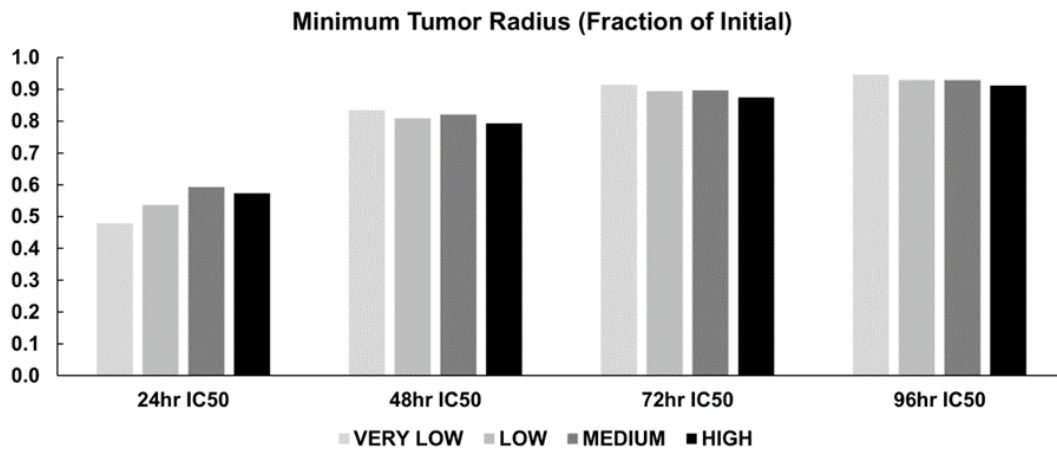


**Figure 10.** Minimum tumor radius achieved during therapy as a function of drug strength and tissue heterogeneity.

## DISCUSSION

This study builds upon previous experimental (England, Priest et al. 2013, England 2015) and modeling work (Curtis, England et al. 2016) to evaluate the effect of vascular density-driven tissue heterogeneity on NSCLC tumor response to cisplatin delivered via 3-layered gold nanoparticles. As such, this work represents a first step towards the development of a principled approach to predict nanotherapy efficacy using patient-tumor-specific characteristics, such as proliferative index and vascular density. Tumors with different intra-tumoral vascular densities (**Figure 1**) were first simulated by varying the oxygen thresholds for hypoxia and necrosis to yield different proportions of proliferating, hypoxic and necrotic tissue (**Figure 2**). Next, using experimentally-obtained data with 3-layered gold nanoparticles loaded with cisplatin (England, Priest et al. 2013, England 2015), the magnitude of the drug effect *in silico* was calibrated for inhibitory drug concentrations to achieve 50% tumor tissue remission over 24, 48, 72, and 96 h (**Figures 5, 6**). The resulting inhomogeneous intratumoral nanoparticle and drug AUC values (**Figure 7**) yield correspondingly heterogeneous tumor regressions (**Figures 8, Figure 10**). This system was then used to determine the expected tumor size based on the fraction of viable tumor tissue and intratumoral vascular density (**Figure 9**).

The results show that vascular tumor density coupled with the drug strength non-trivially influences the nanoparticle uptake and washout, and the associated tissue response. The

drug strength affects the proportion of proliferating, hypoxic and necrotic tissue fractions, which in turn dynamically affect and are affected by the vascular density. A higher drug strength may be able to achieve a stronger tumor regression but only if the intra-tumoral vascular density is beyond a certain threshold (**Figure 9B**). In contrast, drug strengths of lower magnitude may yield similar responses regardless of vascular density. Although regression generally correlated with drug strength, the level of vascular density-driven tissue heterogeneity is shown to modulate this regression, to the point that the difference in drug strength may not matter (**Figure 10**). Since drug strength is a key clinical parameter underlying both response and systemic toxicity, the overall results support the notion that drug strength remains a critical modeling parameter for predictive evaluation. This is consistent with recent modeling work that combined an optimization approach to determine optimal nanoparticle sizes for maximum tumor regression (Chamseddine, Frieboes et al. 2018).

This study establishes a first step towards a more systematic methodology to assess the effect of tumor tissue vascular density on the response to nanotherapy. With experimentally-measurable parameter values, the system could be expanded to evaluate other types of nanoparticles and drugs. Vascular permeability and blood volume could be quantified by positron emission tomography (Chen, Tong et al. 2017). In particular for non-small cell lung cancer (NSCLC), tumor parameters such as vascular density could be measured via imaging or histological analysis (Ma, Ren et al. 2016). Additionally, there exist numerous methods for detecting tumor hypoxia, including the detection of hypoxia-induced proteins through the HIF transcription factor (Zhong, De Marzo et al. 1999, Brahimi-Horn and Pouyssegur 2005). The concept of manipulating the vascular density to achieve improved response (e.g., “vascular normalization” (Jain 2001)), as has been tried

for NSCLC with small molecule tyrosine kinase inhibitors or monoclonal antibodies that target VEGF (Hall, Le et al. 2015), may find further utility depending on the drug strength. Clinically, angiogenesis inhibitors have been shown to lead to improvements in overall survival when combined with standard first line and second line therapy (Hall, Le et al. 2015). In cases where tumor vascular density is determined by the model to be inadequate for a desired level of response, angiogenesis inhibitors may be able to change this density to augment the nanotherapy efficacy.

The interaction between vasculature, cells, nanoparticles, and drug molecules is a complex kinetic process in need of further consideration not only in experimental work but also in future computational modeling and simulation studies. Recently, a vascularized tumor model system was proposed that considers the differences in drug kinetics among various cellular compartments (Curtis, van Berkel et al. 2018). Further studies could combine drug kinetics with a nanoparticle delivery model. The model used herein simulates cell death as an instantaneous process. However, cell cycle dependent drugs such as cisplatin rely on apoptosis and may take several hours before cytotoxic effects are realized (Siddik 2003). Thus, another consideration for future work is to account for the delay in the drug cytotoxic action. Additionally, there are several well characterized drug resistance mechanisms such as decreased intracellular transport, enzymatic deactivation, and alteration in proteins involved in apoptotic pathways (Stewart 2007). These mechanisms could be integrated to create more comprehensive pharmacodynamics models.

## REFERENCES

Bertrand, N., et al. (2014). "Cancer nanotechnology: the impact of passive and active targeting in the era of modern cancer biology." Adv Drug Deliv Rev **66**: 2-25.

Brahimi-Horn, M. C. and J. Pouyssegur (2005). "The hypoxia-inducible factor and tumor progression along the angiogenic pathway." Int Rev Cytol **242**: 157-213.

Chamseddine, I. M., et al. (2018). "Design Optimization of Tumor Vasculature-Bound Nanoparticles." Scientific Reports (**in press**).

Chen, H., et al. (2017). "Quantification of Tumor Vascular Permeability and Blood Volume by Positron Emission Tomography." Theranostics **7**(9): 2363-2376.

Curtis, L. T., et al. (2016). "An interdisciplinary computational/experimental approach to evaluate drug-loaded gold nanoparticle tumor cytotoxicity." Nanomedicine (Lond) **11**(3): 197-216.

Curtis, L. T., et al. (2016). "A Computational/Experimental Assessment of Antitumor Activity of Polymer Nanoassemblies for pH-Controlled Drug Delivery to Primary and Metastatic Tumors." Pharm Res.

Curtis, L. T., et al. (2018). "Pharmacokinetic/pharmacodynamic modeling of combination-chemotherapy for lung cancer." J Theor Biol **448**: 38-52.

Curtis, L. T., et al. (2015). "Computational Modeling of Tumor Response to Drug Release from Vasculature-Bound Nanoparticles." PLoS One **10**(12): e0144888.

Decuzzi, P., et al. (2009). "Intravascular delivery of particulate systems: does geometry really matter?" Pharm Res **26**(1): 235-243.

England, C. G., et al. (2015). "Evaluation of uptake and distribution of gold nanoparticles in solid tumors." Eur Phys J Plus **130**(11).

England, C. G., et al. (2015). "Detection of Phosphatidylcholine-Coated Gold Nanoparticles in Orthotopic Pancreatic Adenocarcinoma using Hyperspectral Imaging." PLoS One **10**(6).

England, C. G., Huang, J., S. James K.T., Zhang, X., Gobin, A.M., Frieboes, H.B. (2015). "Detection of Phosphatidylcholine-Coated Gold Nanoparticles in Orthotopic Pancreatic Adenocarcinoma using Hyperspectral Imaging." PLoS One **10**(6): e0129172.

England, C. G., Miller, M.C., Kuttan, A., Trent, J.O., Frieboes, H.B. (2015). "Release Kinetics of Paclitaxel and Cisplatin from Two and Three Layered Gold Nanoparticles." Eur J Pharm Biopharm **92**: 120-129.

England, C. G., et al. (2013). "Enhanced penetration into 3D cell culture using two and three layered gold nanoparticles." Int J Nanomedicine **8**: 3603-3617.

Frens, G. (1973). "Controlled Nucleation for the Regulation of the Particle Size in Monodisperse Gold Solutions." Nature Physical Sciences **241**: 20-22.

Frieboes, H. B., et al. (2006). Nanotechnology in Cancer Drug Therapy: A Biocomputational Approach. BioMEMS and Biomedical Nanotechnology. M. Ferrari, A. P. Lee and L. J. Lee. New York, Springer-Verlag: 435-460.

Frieboes, H. B., et al. (2013). "A computational model for predicting nanoparticle accumulation in tumor vasculature." PLoS One **8**(2): e56876.

Gao, Y., et al. (2013). "Predictive models of diffusive nanoparticle transport in 3-dimensional tumor cell spheroids." AAPS J **15**(3): 816-831.

Godin, B., et al. (2010). "An integrated approach for the rational design of nanovectors for biomedical imaging and therapy." Adv Genet **69**: 31-64.

Hait, W. N. and T. W. Hambley (2009). "Targeted cancer therapeutics." Cancer Res **69**(4): 1263-1267.



Hall, R. D., et al. (2015). "Angiogenesis inhibition as a therapeutic strategy in non-small cell lung cancer (NSCLC)." Translational Lung Cancer Research **4**(5): 515-523.

Izuishi, K., et al. (2000). "Remarkable tolerance of tumor cells to nutrient deprivation: possible new biochemical target for cancer therapy." Cancer Res **60**(21): 6201-6207.

Jain, R. K. (2001). "Normalizing tumor vasculature with anti-angiogenic therapy: a new paradigm for combination therapy." Nature Medicine **7**(9): 987-989.

Kaddi, C. D., et al. (2013). "Computational nanomedicine: modeling of nanoparticle-mediated hyperthermal cancer therapy." Nanomedicine (Lond) **8**(8): 1323-1333.

Koziara, J. M., et al. (2006). "In-vivo efficacy of novel paclitaxel nanoparticles in paclitaxel-resistant human colorectal tumors." J Control Release **112**(3): 312-319.

Leighl, N. B. (2012). "Treatment paradigms for patients with metastatic non-small-cell lung cancer: first-, second-, and third-line." Curr Oncol **19**(Suppl 1): S52-58.

Li, M., et al. (2010). "Physiologically based pharmacokinetic modeling of nanoparticles." Acs Nano **4**(11): 6303-6317.

Li, M., et al. (2013). "Delineating intracellular pharmacokinetics of paclitaxel delivered by PLGA nanoparticles." Drug Deliv Transl Res **3**(6): 551-561.

Li, M., et al. (2012). "Physiologically based pharmacokinetic modeling of PLGA nanoparticles with varied mPEG content." Int J Nanomedicine **7**: 1345-1356.

Li, M. and J. Reineke (2011). "Mathematical modelling of nanoparticle biodistribution: extrapolation among intravenous, oral and pulmonary administration routes." Int J Nano Biomaterials **3**(3): 222-238.

Ma, E., et al. (2016). "ROI for outlining an entire tumor is a reliable approach for quantification of lung cancer tumor vascular parameters using CT perfusion." Oncotargets and Therapy **9**: 2377-2384.

Macklin, P., et al. (2009). "Multiscale modelling and nonlinear simulation of vascular tumour growth." J Math Biol **58**(4-5): 765-798.

McDougall, S. R., et al. (2006). "Mathematical modelling of dynamic adaptive tumour-induced angiogenesis: clinical implications and therapeutic targeting strategies." J Theor Biol **241**(3): 564-589.

Miele, E., et al. (2012). "Nanoparticle-based delivery of small interfering RNA: challenges for cancer therapy." Int J Nanomedicine **7**: 3637-3657.

Minchinton, A. I. and I. F. Tannock (2006). "Drug penetration in solid tumours." Nat Rev Cancer **6**(8): 583-592.

Nugent, L. J. and R. K. Jain (1984). "Extravascular diffusion in normal and neoplastic tissues." Cancer Res **44**(1): 238-244.

Primeau, A. J., et al. (2005). "The Distribution of the Anticancer Drug Doxorubicin in Relation to Blood Vessels in Solid Tumors." Clinical Cancer Research **11**(24): 8782-8788.

Reichel, D., et al. (2017). "Development of Halofluorochromic Polymer Nanoassemblies for the Potential Detection of Liver Metastatic Colorectal Cancer Tumors Using Experimental and Computational Approaches." Pharm Res **34**(11): 2385-2402.

Siddik, Z. H. (2003). "Cisplatin: mode of cytotoxic action and molecular basis of resistance." Oncogene **22**(47): 7265-7279.

Stewart, D. J. (2007). "Mechanisms of resistance to cisplatin and carboplatin." Crit Rev Oncol Hematol **63**(1): 12-31.

van de Ven, A. L., et al. (2013). "Modeling of nanotherapeutics delivery based on tumor perfusion." New Journal of Physics **15**.

van de Ven, A. L., et al. (2012). "Integrated intravital microscopy and mathematical modeling to optimize nanotherapeutics delivery to tumors." AIP Adv **2**(1): 11208.

Warren, K. E. (2013). "Novel therapeutic delivery approaches in development for pediatric gliomas." CNS Oncol **2**(5): 427-435.

Wu, M., et al. (2014). "The effect of interstitial pressure on therapeutic agent transport: coupling with the tumor blood and lymphatic vascular systems." J Theor Biol **355**: 194-207.

Wu, M., et al. (2014). "The effect of interstitial pressure on therapeutic agent transport: Coupling with the tumor blood and lymphatic vascular systems." Journal of Theoretical Biology **355**: 194-207.

Wu, M., et al. (2013). "The effect of interstitial pressure on tumor growth: Coupling with the blood and lymphatic vascular systems." J Theor Biol **320**: 131-151.

Zhong, H., et al. (1999). "Overexpression of hypoxia-inducible factor 1alpha in common human cancers and their metastases." Cancer Res **59**(22): 5830-5835.

## CURRICULUM VITAE

NAME: Hunter Allan Miller

ADDRESS: Department of Pharmacology and Toxicology  
505 S Hancock St.  
University of Louisville School of Medicine  
Louisville, KY 40202

### EDUCATION &

TRAINING: B.S. Chemistry/Biochemistry  
Murray State University  
2011-2016

### PUBLICATIONS:

HA Miller, HB Frieboes. Evaluation of Cancer Nanotherapy as a Function of Tumor Vascularization. Presentation at Biomedical Engineering Society annual meeting Atlanta, GA (Oct. 2018)

HA Miller, HB Frieboes. Evaluation of drug-loaded gold nanoparticle cytotoxicity as a function of tumor tissue heterogeneity. *Annals of Biomedical Engineering* 2018 (in review)

LB Sims\*, HA Miller\*, ME Halwes, JM Steinbach-Rankins, HB Frieboes. Modeling of nanoparticle transport through the vaginal epithelium for the treatment of infectious diseases. *Eur J Pharmacol Pharmaceutics* 2018 (in review). \*Joint first authorship

HA Miller, HB Frieboes. Simulation of the effect of tumor vessel density on drug loaded gold nanoparticle efficacy. Poster presentation at Research Louisville (2017)